TECHNICAL ARTICLE

Effect of Vanadium on Wear and Corrosion Resistance of Fe-C-Cr Hardfacing Coatings

Nilay Çömez

The objective of the study was to investigate the effect of vanadium on wear and corrosion resistance in Fe-Cr-C hardfacing alloy. The hardfacing coatings were deposited onto the S235JR steel using metal arc welding method. The addition of vanadium gave rise to the formation of VC and V_2C carbides. The increase in vanadium and the decrease in carbon content reduced the size of primary carbides and carbide volume fraction. However, vanadium increased the microhardness of the primary carbide. The vanadium-free coating showed maximum hardness and wear resistance while having the maximum corrosion rate. The optimal vanadium content was 2% by weight to achieve a coating as wear-resistant as Fe-Cr-C alloy without vanadium. Scratches due to abrasive wear and fracture of the primary carbide were observed on the worn surface of the coatings. The addition of vanadium raised the corrosion resistance 3-4 times.

1. Introduction

Hardfacing is a cost-effective metal deposition technique that extends the service life of engineering components such as in mining, crushing, grinding, and agriculture equipment by generating a wear and corrosion resistant coating (Ref 1-3). Hardfacing alloys can be applied to metal surfaces by various techniques like laser cladding, plasma transferred arc, gas metal arc, submerged arc, oxyacetylene, and shielded metal arc welding methods (Ref 4-6).

The wear resistance of Fe-Cr-C-based hardfacing coatings derives from the existence of hard and large primary M_7C_3 carbides and eutectic carbides dispersed in the iron-based matrix material (Ref 7). Additionally, the existence of strong carbide former elements such as Mo, Ti, W, V, and Nb improves the tribological properties of the coating by forming carbide precipitation and enhancing the properties of matrix (Ref 5, 8). Abrasion resistance of the coatings relies on the increased hardness (Ref 9). The formation of primary and secondary carbides in a metallic matrix material generates a composite structure. In situ formed carbides act as reinforcement. Hence, its ratio in the matrix material affects the tribological properties of coatings. In a recent study about the composite structures, it was noticed that the wear resistance tends to increase up to a threshold percentage of the reinforcement particles (Ref 10).

Günther and Bergmann (Ref 4) pointed out that vanadium carbide reinforced hardfacing alloys become even more impor-

tant for superior abrasion and impact resistance. Several studies have focused on the effect of vanadium on the tribological properties of Fe-C-Cr hardfacing alloys. Jiang et al. (Ref 11) investigated hardfacing alloys containing four different vanadium contents in terms of microstructural changes and wear resistance. Similarly, Qi et al. (Ref 12) proved the formation of VC with an increasing vanadium content and indicated that the vanadium additive is beneficial for the wear resistance of the hardfacing coating. Singla et al. (Ref 13) produced Fe-Cr-C-V coatings using the shielded metal arc welding (SMAW) method and reported that increased vanadium content increased the hardness and adhesive wear resistance. Lai et al. (Ref 14) added vanadium to Fe-Cr-C alloy between 0 and 2.39 percent by weight. They observed the formation of fibrous V_4C_3 with a vanadium concentration of 0.93 wt.%. References on the effect of vanadium on the wear resistance of hardfacing coatings can be further increased. However, studies on the effect of vanadium on corrosion resistance are limited in the literature. The purpose of this study is to reveal the effect of vanadium and carbon content not only on tribological and microstructural properties but also on the corrosion resistance of the coating.

2. Materials and Method

2.1 Welding Procedure of Hardfacing Coatings

Fe-C-Cr and Fe-C-Cr-V hardfacing alloys were deposited on a 5 mm thick S235JR steel. Ferrochromium and ferrovanadium were added to the solid wire with an automated powder supply unit during the arc welding process (Table 1). The mixture of ferroalloys was stored in the chamber of the powder supply unit. The powder mixture was transferred to the weld pool with a pipe connected to the powder feeding regulator of the chamber. Coatings consist of a mixture of 70 wt.% of ferroalloy powder and 30 wt.% of solid wire. The chemical compositions of wire and ferroalloys are shown in Table 2. The chemical compositions of the coatings were determined by optical emission spectroscopy (Table 3).

Nilay Çömez, Department of Metallurgical and Materials Engineering, Manisa Celal Bayar University, Manisa, Turkey; and Department of Mechanical Engineering, Ege University, İzmir, Turkey. Contact e-mail: nilay.comez@cbu.edu.tr.

2.2 Microstructural Investigations

Metallographic examinations of the coatings were performed by an optical microscope and SEM. The samples were etched with Kalling's solution (33 ml H_2O, 1.5 g $CuCl_2$, 33 ml methanol ve 33 ml HCl). The volume fraction of microstructure constituents was calculated by the Clemex software (Fig. 1). Chemical compositions of matrix and carbides were determined by SEM–EDX analysis and the types of carbides were detected by XRD analysis. The coating surfaces were scanned with XRD between 30 and 90°.

2.3 Hardness and Wear Tests

The macro Vickers hardness test was applied to the surface of the hardfacing coating under 20 kgf loads according to ASTM: E-384 standard. The macrohardness measurements were taken from different zones of the top surface of the sample with an area of 25×25 mm^2. In addition, hardness measurements were taken along the cross section of the coating under a load of 1 kgf to detect the dilution effect. The hardness of the microconstituents of the coatings was determined by the Vickers indenter at a load of 50 gf (Fig. 2).

Ball-on-disk wear test of the hardfacing coatings was performed in a dry environment at a load of 10 N and at ambient temperature (25 ± 3 °C) with a CMS Instruments tribometer. The wear test was applied on a sample with an area of 25×25 mm^2 for each coating. An alumina ball with a diameter of 6 mm was used as a counterpart. The sliding distance and radius of the wear track were set to 1500 m and 4 mm, respectively. The worn surface topography was measured with a Mitutoyo profilometer to calculate the volumetric loss of material. The topography measurements of the wear track were accomplished along eight different lines of the wear track for each sample.

2.4 Corrosion Test

The corrosion test was performed with Metrohm Dropsens Potentiostat/Galvanostat equipment in 0.4 M NaCl solution. The corrosion cell is composed of a 75 ml NaCl solution, an Ag/AgCl reference electrode, a graphite electrode, and the sample as a working electrode. One sample with an exposure area of 16 mm^2 was used in the corrosion test for each coating. Each sample was immersed in a solution of NaCl for 60 s to stabilize the open circuit potential (OCP). The scan rate of the corrosion test was set to 0.001 V/s. Tafel curves were plotted from − 1 to 0.3 V. The corrosion rate was computed using the Dropview software according to the Tafel extrapolation methodology. Corroded surfaces were investigated in SEM.

3. Results and Discussion

3.1 Microstructure

The microstructure of hardfacing coatings consists of rod-like primary carbides with hexagonal cross section and secondary carbides dispersed in the matrix (Fig. 3). The XRD result of FeCr-V0 without vanadium addition showed that the carbide type is M_7C_3 (M: Fe, Cr) (Fig. 4a). SEM–EDX analysis revealed that vanadium promoted the formation of M_7C_3 primary carbides consisting of V, Cr, and Fe. A small amount of vanadium was dissolved in the matrix (Fig. 5). In addition to M_7C_3 and $M_{23}C_6$ carbides, V_2C and VC carbides with a low peak intensity were observed in vanadium added coatings (Fig. 4b). The XRD analysis of FeCr-V8 shows the formation of VC and V_2C carbides whereas FeCr-V12 only has the VC peak. The increase in vanadium content resulted in VC formation which is thermodynamically more stable than V_2C, as stated by Wu et al. (Ref 15). FeCr-V0 has only the formation of M_7C_3 whereas coatings with vanadium contain both $M_{23}C_6$ and M_7C_3. The addition of vanadium led to a reduction in carbon content. The decrease in carbon induces the formation of $M_{23}C_6$ as shown in Fe-Cr-C diagram (Ref 16).

Table 1   Welding parameters

Voltage, V	28–30
Current, A	350
Welding speed, mm/min	140
Oscillation width, mm	40

Table 2   Chemical compositions of solid wire and ferroalloys (wt.%)

Element	V	C	Si	S	P	Cr	Mn	Fe
Massive wire	…	0.08	0.8	…	…	…	1.45	Rest
Ferrovanadium	57.5	0.1	1.5	0.017	…	…	…	
Ferrochromium	…	7.27	0.516	0.061	0.01	67.84	…	

Table 3   Chemical compositions of coatings by optical emission spectroscopy and the content of powder mixture (wt.%)

| Sample | V | Spectral analysis | | | | | | | Powder mixture | |
		Cr	C	Mn	Si	Other	Fe	FeCr	FeV
FeCr-V0	…	47.5	3.85	0.49	1.78	0.82	Rest	100	…
FeCr-V8	2.02	43.8	2.73	0.56	2.02	0.75		92	8
FeCr-V10	2.84	41.05	2.5	0.51	2.3	0.74		90	10
FeCr-V12	3.5	39.93	2	0.53	2.1	0.89		88	12

The microstructure of the coating/substrate interface is shown in Fig. 3. The interface includes martensite due to the high solidification rate of the highly alloyed coating. A thermal gradient occurs between the molten material and the substrate at ambient temperature. Due to the high thermal gradient, the coating exhibited a planar growth at the beginning of the solidification (Fig. 3). Deng et al. (Ref 17) stated that in the dilution zone, a planar growth pattern can be observed near the substrate-coating interface due to the high-temperature gradient and small structural supercooling. Dilution is a commonly encountered issue in hardfacing coatings. It depends on the diffusion of alloying elements in the coating to the substrate and the amount of molten substrate mixing with the coating (Ref 18). Dilution is defined as the ratio between the molten area of the substrate and the total molten area (Ref 19). Although it affects the mechanical, tribological, and corrosion properties of the coating (Ref 20), it ensures a functionally graded structure between a hard, brittle coating and a relatively soft, tough substrate. All coatings exhibited a hypereutectic microstructure including primary carbides and eutectic of matrix + secondary carbides. However, the hypereutectic microstructure evolved into a hypoeutectic structure near the coating/substrate interface as a result of dilution. The microstructure of the dilution zone of FeCr-V12 shows a hypoeutectic structure composed of a dendritic matrix structure and secondary carbide precipitations among these dendrites (Fig. 3f). Reduced vanadium content and increased amount of carbon and chromium caused the secondary carbides between the dendrites to grow in the dilution zone (Fig. 3e and Fig. 3f). Moreover, FeCr-V0 consists of small-sized primary carbides in addition to the eutectic of matrix + secondary carbides in the dilution zone (Fig. 6b).
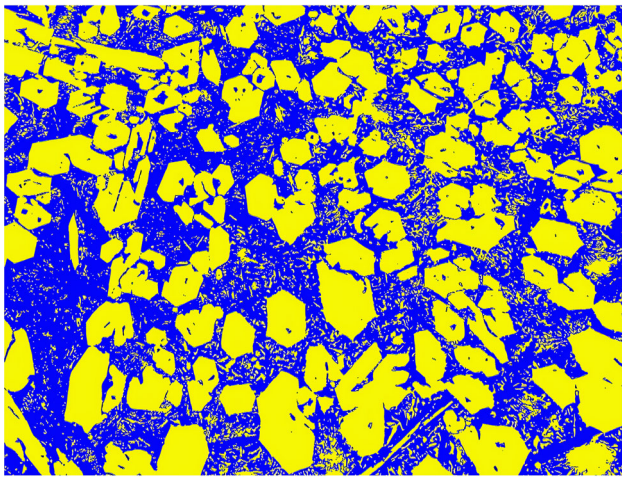

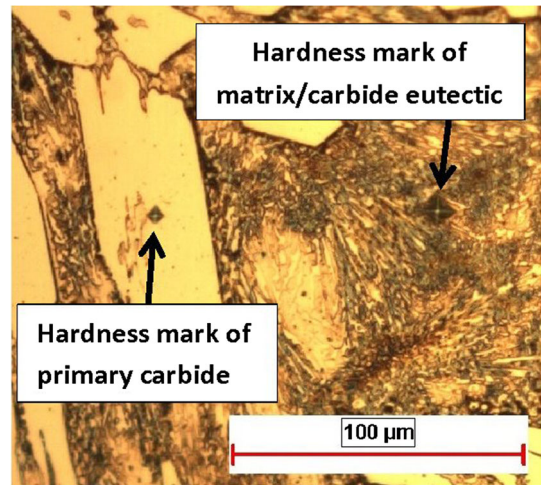**Fig. 1** Carbide volume fraction analysis of FeCr-V0 (dark phase: matrix, light phase: carbide)

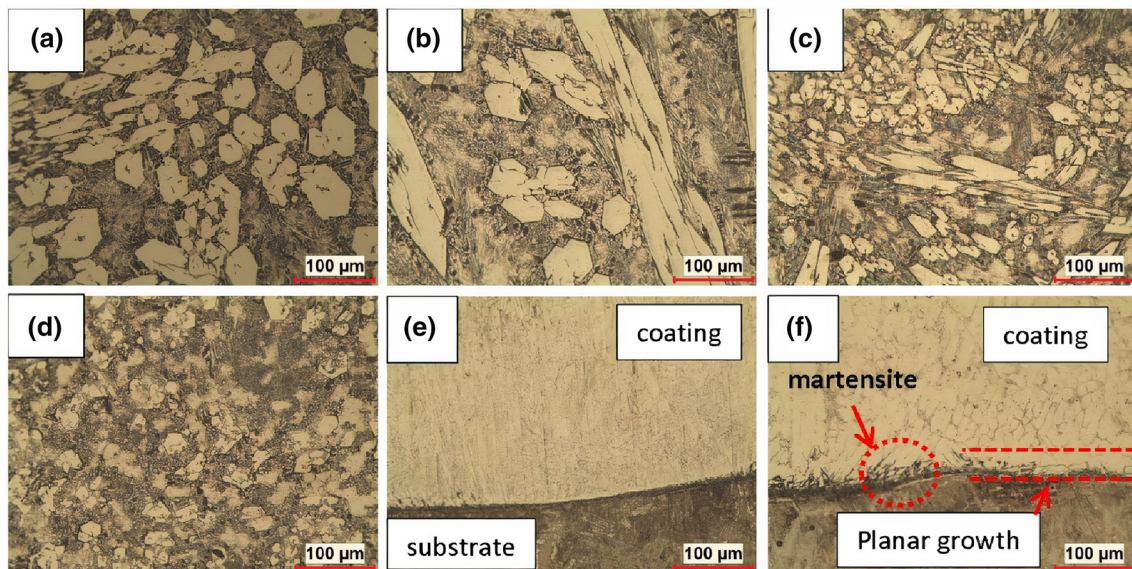**Fig. 2** Microhardness measurement of microconstituents

Fig. 3 Microstructure of hardfacing coatings: (a) FeCr-V0, (b) FeCr-V8, (c) FeCr-V10, (d) FeCr-V12, and coating/substrate interface: (e) FeCr-V8, (f) FeCr-V12
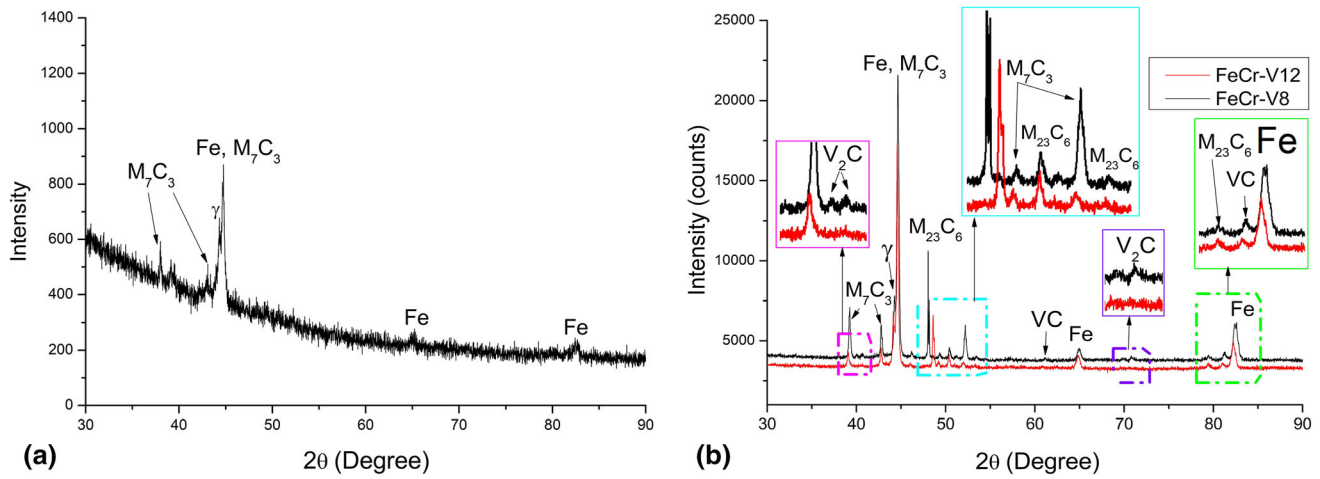
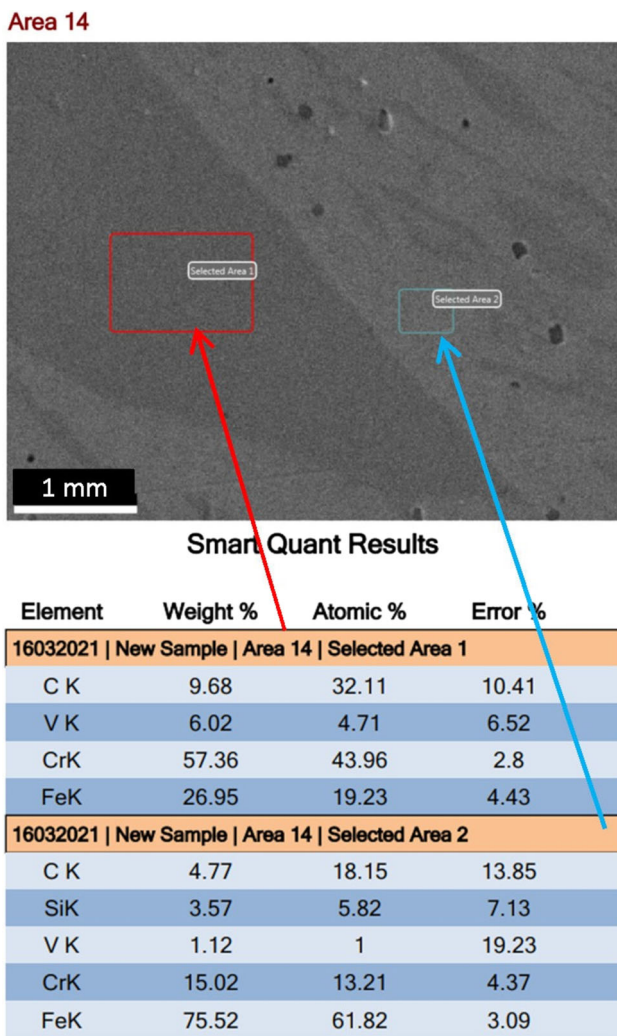**Fig. 4** XRD analysis of: (a) FeCr-V0, (b) FeCr-V8 and FeCr-V12

Fig. 5 SEM–EDX analysis of FeCr-V8

Fig. 6 Hardness survey of the hardfacing coatings

According to the microhardness survey, dilution is more distinct for FeCr-V0. The surface hardness of FeCr-V0 is above 800 HV, whereas the hardness is below 600 HV in the diluted zone 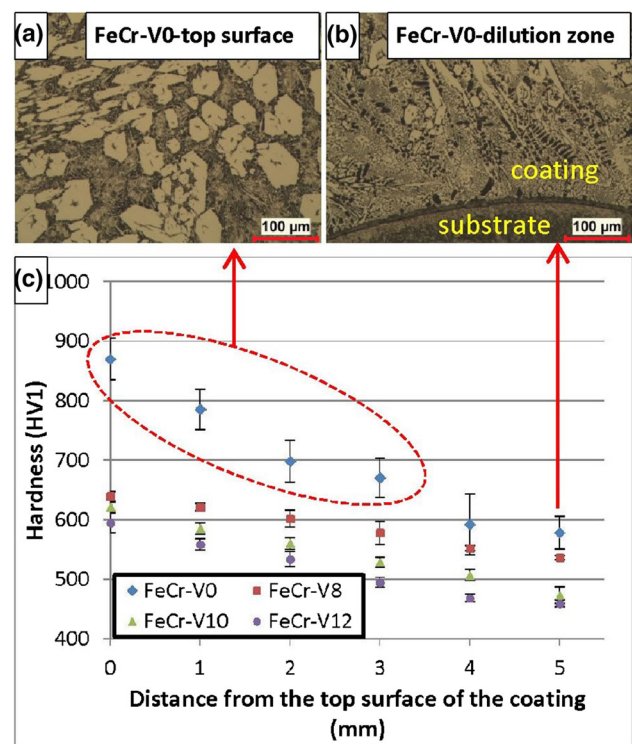near the substrate. The reduction in the amount of primary carbide in the dilution zone resulted in a sharp decrease in hardness (Fig. 6c).

The obvious effect of increasing vanadium and decreasing carbon is the refinement of the primary carbide size (Fig. 3). When the vanadium content exceeded 2 wt.%, the refinement of the primary carbides became significant. Wang et al. (Ref 21) reported that adding vanadium moves the eutectic point to the right and restricts the temperature range of the "liquid + M_7C_3" zone. Consequently, primary carbides have less time to grow. Although 2 wt.% vanadium did not have an obvious effect on primary carbide size, it caused a sharp decrease in CVF (Fig. 3 and Fig. 7a). Sabet et al. (Ref 22) stated that the increasing amount of carbon in hardfacing alloys increases the hardness by supporting the CVF. The addition of
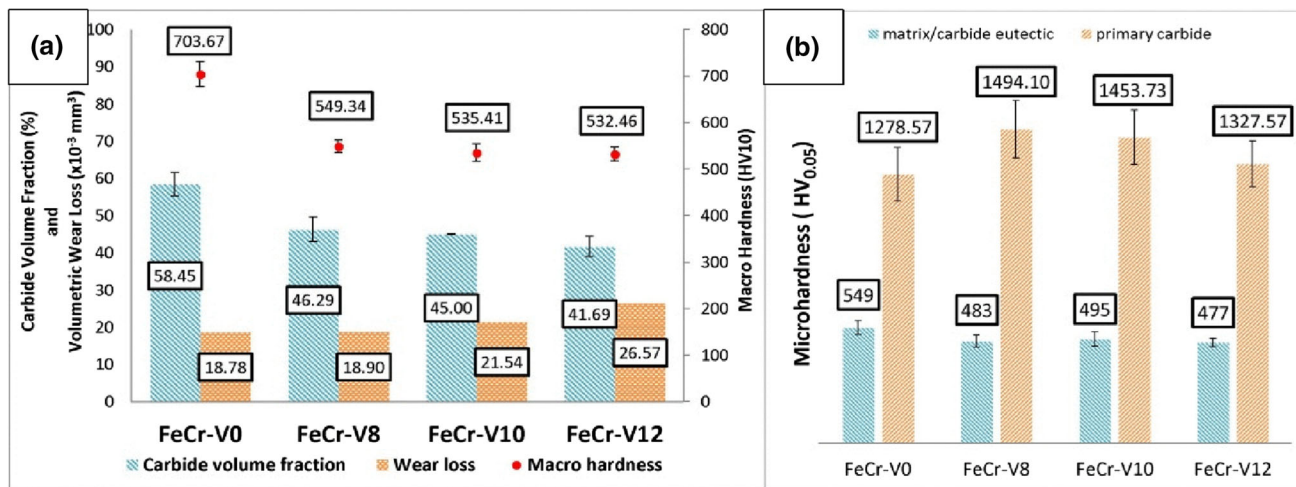
Fig. 7 (a) Correlation between hardness, wear loss, and carbide volume fraction, (b) microhardness of matrix/carbide eutectic and primary carbide
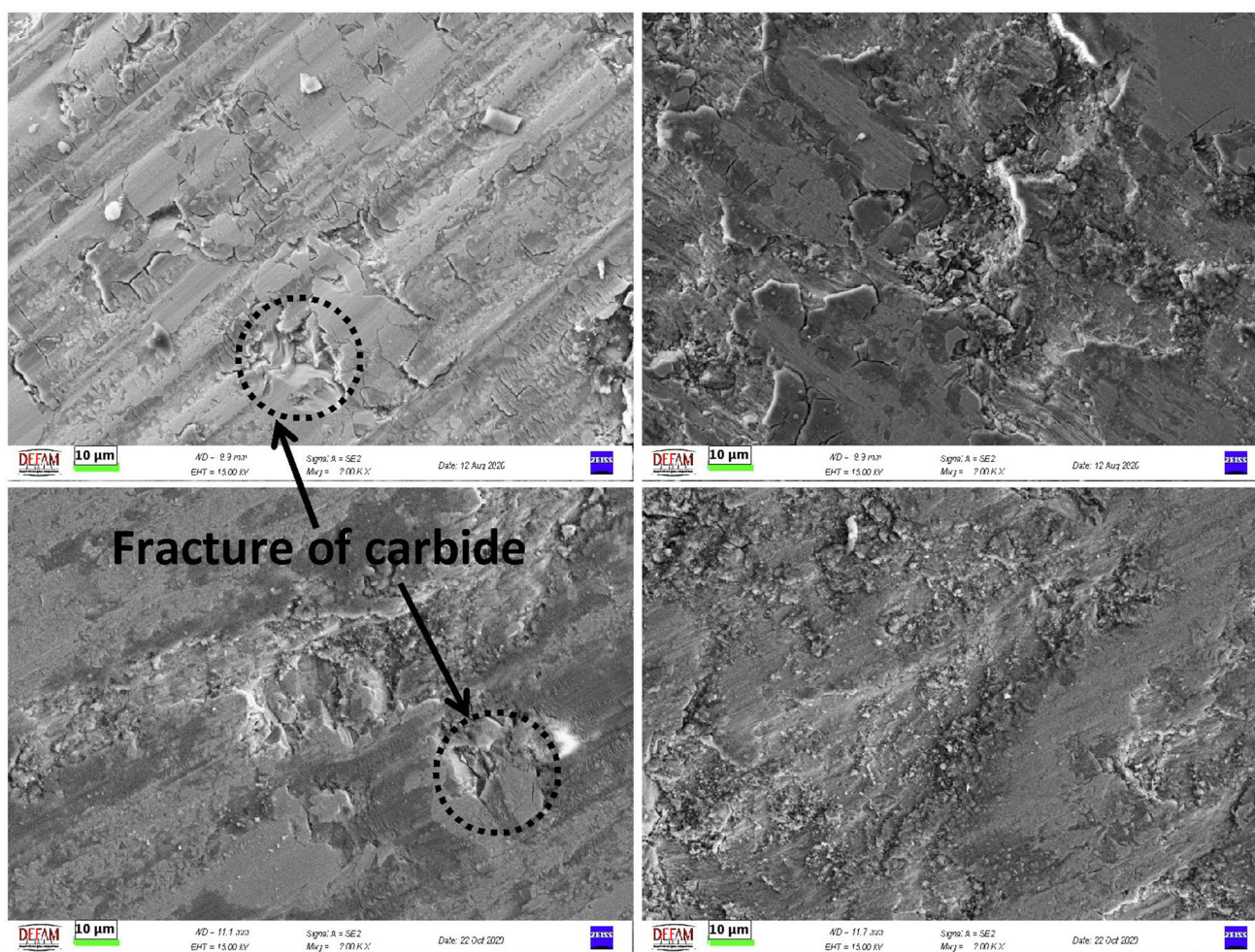

Fig. 8 Worn surface of hardfacing coatings: (a) FeCr-V0, (b) FeCr-V8, (c) FeCr-V10, (d) FeCr-V12

ferrovanadium reduced the amount of both chromium and carbon, and resulted in a 20-30% decrease in CVF. However, the increase in vanadium contributed to the formation of VC carbide, although it was not detected by microstructural investigations. Günther and Bergmann (Ref 4) produced a hardfacing coating including 12 wt.% V and 2.7 wt.% C, and observed dispersion of nanosized vanadium carbides. But in this study, the maximum vanadium content is 3.5 wt.%. Consequently, the formation of a low concentration of nanoscale VC/V_2C was proven with XRD analysis (Fig. 4b).

3.2 Correlation between Hardness and Wear Resistance

The correlation between hardness, wear loss, and CVF of the coatings is given in Fig. 7(a). Minimum wear loss was observed in FeCr-V0 due to its high macrohardness and CVF.
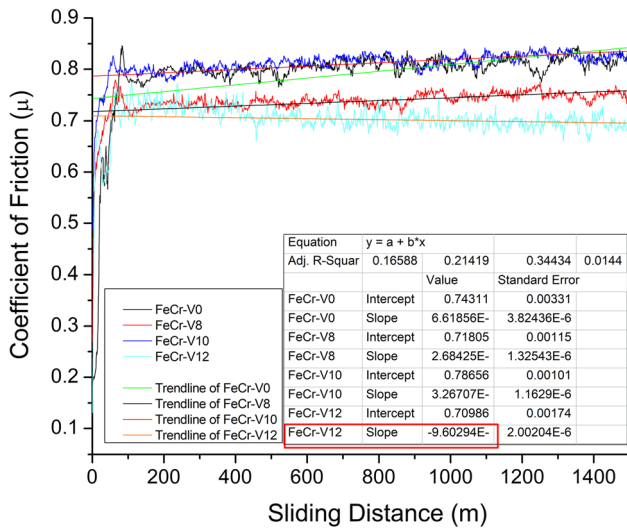

Equation	y = a + b*x			
Adj. R-Squar	0.16588	0.21419	0.34434	0.0144
		Value	Standard Error	
FeCr-V0	Intercept	0.74311	0.00331	
FeCr-V0	Slope	6.61856E-	3.82436E-6	
FeCr-V8	Intercept	0.71805	0.00115	
FeCr-V8	Slope	2.68425E-	1.32543E-6	
FeCr-V10	Intercept	0.78656	0.00101	
FeCr-V10	Slope	3.26707E-	1.1629E-6	
FeCr-V12	Intercept	0.70986	0.00174	
FeCr-V12	Slope	-9.60294E-	2.00204E-6	

Legend:
- FeCr-V0
- FeCr-V8
- FeCr-V10
- FeCr-V12
- Trendline of FeCr-V0
- Trendline of FeCr-V8
- Trendline of FeCr-V10
- Trendline of FeCr-V12

Fig. 9 Coefficient of friction-sliding distance graphs of the coatings

The hardness of the coatings tended to decrease with the decrease in CVF and the formation of $M_{23}C_6$ (Fig. 7a). Durmuş et al. (Ref 23) reported that the hardness of the coatings depends on the volume fraction of primary carbides and the microstructure. A reduction in hardness and CVF led to an increase in wear loss. Although the addition of 2 wt.% vanadium reduced macrohardness by approximately 22%, it resulted in an increase in volumetric material loss of only 1% compared to FeCr-V0. The competitive wear resistance of FeCr-V8 with FeCr-V0 can be attributed to a number of factors such as the formation of nanosized VC, V_2C, and $M_{23}C_6$ (Fig. 4b); increased hardness of primary carbides (Fig. 7b); and increased toughness through reduced hardness of the matrix. The nanosized VC and V_2C carbides dispersed in the matrix material ensure the protection of the matrix without decreasing its fracture toughness. Furthermore, the formation of $M_{23}C_6$ has a positive influence on the wear resistance by balancing the fracture toughness and hardness of the coating. As many studies point out (Ref 24-26) the primary M_7C_3 improves wear resistance. However, hard, brittle M_7C_3 carbide blocks with a hard matrix can increase the intensity of wear by cracking and spalling (Ref 27). As stated by Wang et al. (Ref 7), and Wang and Li (Ref 28), M_7C_3 reduces the fracture toughness of the coating and flakes off from the matrix due to the lattice mismatch stress between the interface of the hard primary carbide and softer matrix. Besides, the primary M_7C_3 can easily
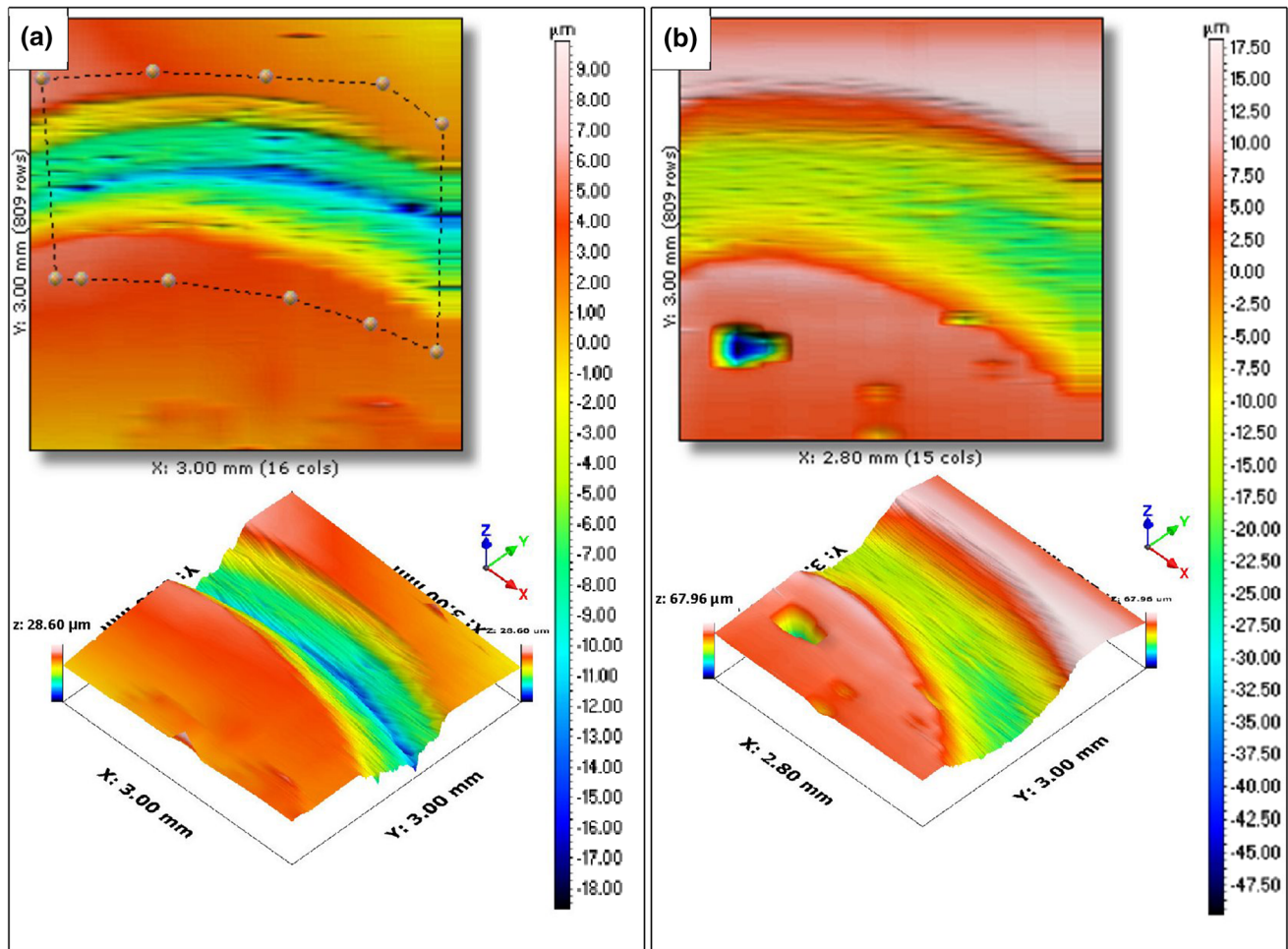

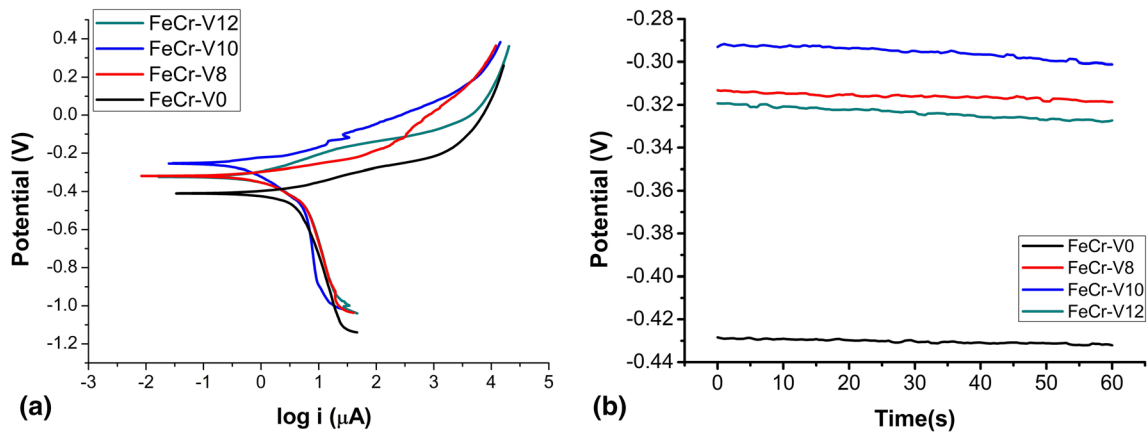**Fig. 10** 3D profilometer images of (a) FeCr-V8 and (b) FeCr-V12

Fig. 11 (a) Tafel curves and, (b) open circuit potential of hardfacing coatings

Table 4 Corrosion test results of coatings

Sample	Ecorr, V	Icorr, μA	Ba, V/dec	Bc, V/dec	Rp, kOhm	Corrosion rate, mm/year
FeCr-V0	− 0.40964	2.06870	0.27547	0.08447	13.56864	0.75
FeCr-V8	− 0.31894	0.89606	0.18106	0.05680	20.95131	0.26
FeCr-V10	− 0.28536	0.76626	0.22101	0.11313	42.40323	0.19
FeCr-V12	− 0.31663	0.82801	0.17240	0.10222	33.65298	0.23

undergo cracking during the cyclic load of the ball-on-disk wear test (Fig. 8a and c). The maximum microhardness in secondary carbide/matrix eutectic was obtained in FeCr-V0. Consequently, this coating became more sensitive to the formation of micro-cracks due to the cyclic load of the wear test. Tabrizi et al. (Ref 29) reported that the higher microhardness could generate more micro-cracks.

Based on the SEM–EDX analysis, vanadium was preferentially dissolved in M_7C_3 rather than in the matrix phase (Fig. 5). Therefore, the hardness of the primary M_7C_3 of Fe-C-Cr-V alloys was higher than that of FeCr-V0. Similarly, Wang and Li (Ref 30) observed that the added vanadium and tungsten were dissolved in the M_7C_3 primary carbides and increased their hardness by solution hardening. The maximum microhardness of the primary carbides was observed in FeCr-V8. The superior wear resistance of the FeCr-V0 coating lies on the amount of CVF and its high macrohardness. Although the FeCr-V8 coating has a lower CVF than FeCr-V0, its volumetric material loss is almost equal to the material loss of FeCr-V0 because of its higher microhardness of the primary carbide. As well as the mechanical properties of the primary carbides, the hardness of the matrix material, the morphology, and size of the carbides determine the type of material loss (Ref 31). The addition of vanadium reduced the carbon content of the coating. Moreover, due to the greater carbide forming tendency of vanadium in comparison with chromium leads to the formation of vanadium carbides (Ref 30, 32). As a result, the carbon content of the matrix is reduced due to the carbon consumption by vanadium and chromium. A reduction in carbon forms a softer matrix with a higher fracture toughness. During the wear test, a softer matrix can be easily deformed and generate a strain hardening effect which improves the wear resistance of the coating. However, a further decrease in CVF and bulk hardness

of the coating—as observed in FeCr-V10 and FeCr-V12—weakens these aforementioned effects.

Worn surfaces of coatings indicate the preponderance of abrasive wear. Continuous scratches were observed on the worn surfaces of all coatings. In addition, worn surfaces include cracking and fracture of primary carbides (Fig. 8). Figure 9. shows that the coefficient friction values (COF) of the coatings in the steady-state friction are between 0.7 and 0.8. All coatings reached the steady-state sliding after 100 m sliding distance. COF of FeCr-V12 exhibited a decreasing trend (negative slope) by the sliding distance, while the other coatings exhibited an increasing trend in COF (positive slope). The contact area has a great influence on the wear mechanisms (Ref 29). During grinding and polishing step of the wear test samples, matrix phase is expected to be abraded more than the carbides. Consequently, after sample preparation the carbides generate peaks while the matrix generates valleys between the carbides. During the wear test it is thought that the counterpart contacted with the carbides first. Hence, the high carbide content of the FeCr-V0 may result in an increase in the real contact area which increased the COF. In contrast, FeCr-V12 has the minimum carbide volume fraction which provides less protection for the softer matrix material. During the material loss from the matrix material including Cr, formation of oxides such as Cr_2O_3 can be encountered. As stated by Tabrizi et al. (Ref 33), oxide formation decreases the COF due to the self-lubrication nature of oxides. FeCr-V12 with a lower carbide volume fraction and lower macro/microhardness values can undergo plastic deformation easier than other coatings. Consequently, it was expected that FeCr-V12 generated wear debris with a higher amount of oxides which resulted in a COF with a decreasing trendline. As can be seen from the SEM image (Fig. 8d) of worn surface of FeCr-V12, the scratches are not as distinct as the worn surface of other coatings. 3D profilometer images of
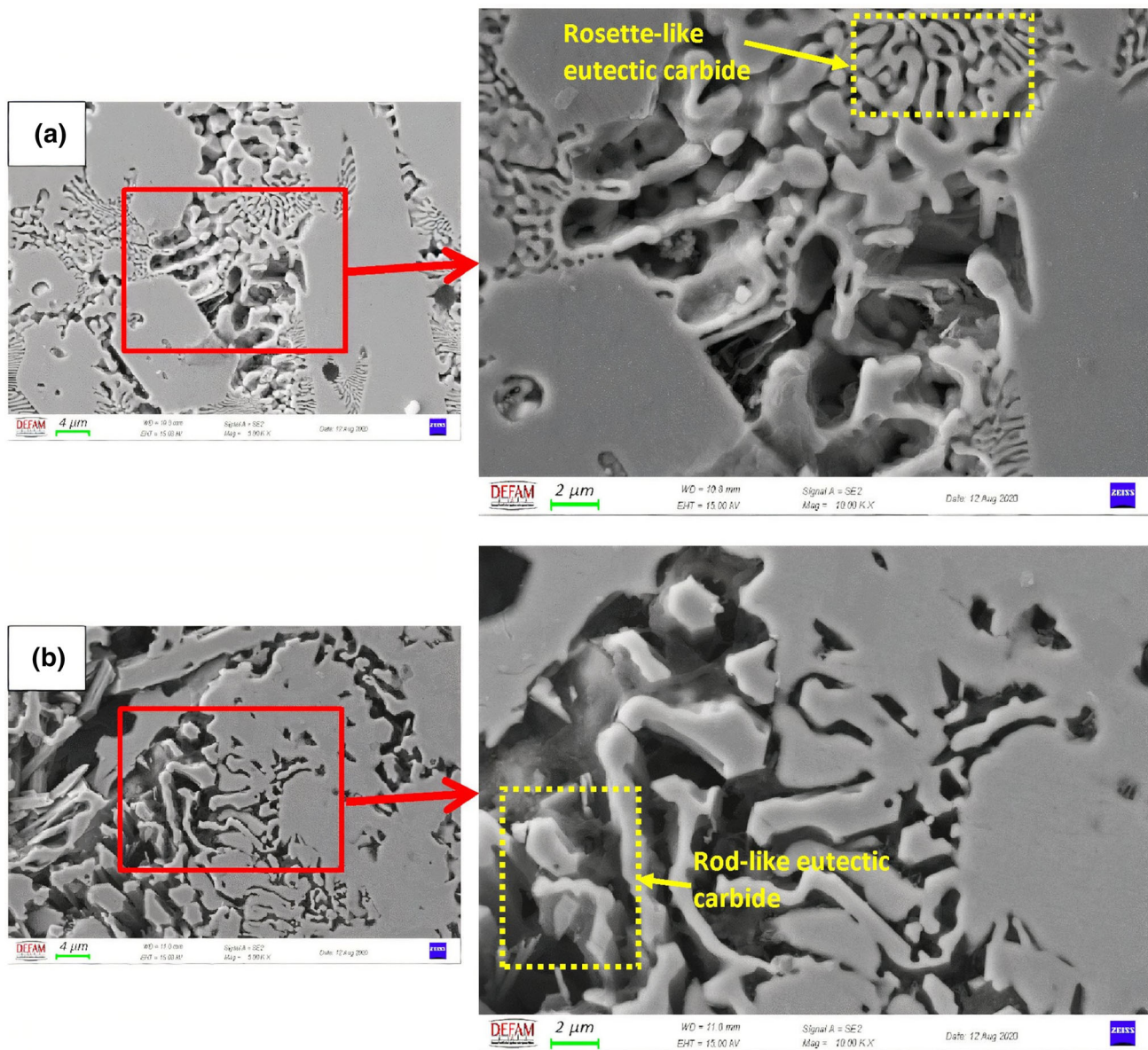
Fig. 12 Corroded surface of coatings: (a) FeCr-V0 and (b) FeCr-V10

worn surface of FeCr-V12 and FeCr-V8 clearly present the difference in wear mechanisms of these coatings. Worn surface of FeCr-V12 exhibited a smooth surface topograhy depending on giving the way of adhesive and abrasive wear to oxidative wear (Fig. 10b) while the wear track of FeCr-V8 included sharp and deep scratches of abrasive wear mechanism (Fig. 10a). It can be concluded that decreasing the carbide content and hardness supported the plastic deformation of the matrix material and induced the oxidative wear in addition to adhesion and abrasion.

3.3 Corrosion Rate

The Tafel curves and the OCP of the coatings are given in Fig. 11. The OCP can be used to predict the corrosion resistance of coatings. As expected from the OCP results, the maximum corrosion rate was observed in FeCr-V0 which has the most negative corrosion potential. In contrast, FeCr-V10 with less negative OCP and minimum potential exhibited the minimum corrosion rate (Fig. 11b and Table 4). Günen et al. (Ref 34) reported that the alloys with less negative OCP exhibit a higher corrosion resistance. Furthermore, Ahmad (Ref 35) stated that the material with a more negative potential tends to dissolve more than that of material with less negative potential. Similarly, polarization resistance (Rp) gives an insight into the oxidation resistance of a material (Ref 36). FeCr-V10 has the minimum corrosion rate owing to its high oxidation resistance, in the other words "polarization resistance" (Table 4). A significant difference was not observed in the corrosion rates of coatings with vanadium. However, a small change in the corrosion rate of these coatings can be explained by the silicon content (Table 2). Kocaman et al. (Ref 37) stated that the silicon content of the matrix promotes the corrosion resistance of the coatings.

Zhang et al. (Ref 38) revealed that carbides have a higher free corrosion potentials than that of matrix. The difference in corrosion potential between the carbide and the matrix explains

the dissolution of the matrix phase. Because the potential difference indicates the tendency of corrosion as described above: The more negative the potential the more tendency of corrosion.

This study revealed that decreased CVF enhanced the corrosion resistance of hardfacing coatings. The corrosion rates of coatings with vanadium are about 3–4 times lower than that of FeCr-V0 (Table 4). But some studies published in the literature suggest that increased CVF increases corrosion resistance. For instance, Azimi and Shamanian (Ref 39) reported that the higher amount of M_7C_3 leads to more noble potential for coating. Similarly, Chang et al. (Ref 40) stated that an increase in the amount of primary $(Cr,Fe)_7C_3$ would enhance corrosion resistance. However, a galvanic coupling takes place between the anodic matrix and the cathodic carbides (Ref 41). This is why a large amount of M_7C_3 carbides extends the matrix/carbide interface area and can increase the corrosion rate by favoring galvanic corrosion. Gou et al. (Ref 41) reported that the boundaries between the eutectic carbides and the matrix should be reduced in an attempt to decrease the interphase corrosion between the eutectic carbides, thus improving corrosion resistance. The microstructure of FeCr-V0 consists of large M_7C_3 primary carbides and rosette-like eutectic carbides (Fig. 12a) as is also observed by Bedolla-Jacuinde et al. (Ref 42). In contrast, the addition of vanadium led to the formation of rod-like eutectic carbides (Fig. 12b) which reduce the area of the matrix/carbide interface. The sinuous structure of the rosette-like eutectic carbides in FeCr-V0 increased the area of interface between the carbides and the matrix. As a consequence, the activity of galvanic corrosion expanded in a large area and induced the dissolution of the matrix in the nanoscaled channels of the rosette-like eutectic carbides and around the primary carbides (Fig. 12a). In addition, the coherency between the crystal structures of the matrix and the carbides may have an influence on the corrosion behavior of the composite structured hardfacing coatings. VC (Ref 43), $M_{23}C_6$ (Ref 44), and the iron-based matrix phase have a cubic structure whereas M_7C_3 (Ref 44) and V_2C (Ref 45) carbide have orthorhombic crystal structure. Vanadium addition resulted in the formation of $M_{23}C_6$ carbide which has a cubic structure such as the iron-based matrix. Hence, a significant reduction in the corrosion rate was observed due to the formation of $M_{23}C_6$ carbide although the chromium content decreased. Altun and Sen (Ref 46) stated that the harmony between the lattice structures of the phases in a microstructure can improve the corrosion resistance. Considering the coatings with vanadium, it can be expressed that the formation of V_2C with orthorhombic structure can be desired for wear resistance. Because the mismatch between the crystal structures of V_2C and the matrix can provide higher lattice strains, consequently the structure can resist dislocation motions more during the wear test. However, the existence of V_2C is not desired in the point of view of corrosion resistance due to the its incoherent crystal structure with the cubic matrix. V_2C peaks were observed in FeCr-V8 which has the maximum corrosion rate among the coatings with vanadium. Superior corrosion resistance was observed in FeCr-V10 which has most probably a good combination of chromium content and VC. A further reduction in chromium content in FeCr-V12 deteriorate the corrosion properties of the coating in despite of the existence of VC instead of V_2C. Even so, as it was stated before, the percentage of vanadium in the coating did not generate a distinct difference in the corrosion rates of these coatings in comparison with the corrosion rate of coating without vanadium.

4. Conclusions

In this study, the effect of vanadium and carbon contents of Fe-Cr-C hardfacing alloy was investigated in terms of microstructure, hardness, wear, and corrosion resistance properties. The findings can be summarized in the following terms:

1. Hexagonal-shaped M_7C_3 primary carbide showed dominance in vanadium-free coating whereas $M_{23}C_6$, VC, and V_2C carbides occurred in addition to M_7C_3 in coatings, including vanadium. The addition of vanadium altered the morphology of the eutectic carbides. The vanadium-free coating exhibited a rosette-like eutectic carbide structure whereas the addition of vanadium led to the formation of rod-like eutectic carbides.
2. The increase in vanadium resulted in a decrease in carbon content, which resulted in a decrease in CVF and in the size of the primary carbides. M_7C_3 carbide strongly affects the macrohardness of the coating. However, hardness is not the only factor determining wear resistance. Although the maximum hardness and minimum material loss were observed in the vanadium-free coating, the addition of vanadium by about 2% resulted in almost the same amount of material loss due to an increase in microhardness of the M_7C_3 and a tougher matrix.
3. Corrosion resistance enhanced by adding vanadium and a reduction in the carbon content of the coating. The vanadium-free coating showed the maximum corrosion rate. The addition of vanadium reduced the corrosion rate 3 to 4 times. The reduced surface area of the carbide/matrix interface retarded the galvanic corrosion and increased the corrosion resistance. A change in the amount of vanadium had no significant effect on corrosion.

References

1. S. Balaguru, M. Abid, and M. Gupta, Investigations on Different Hardfacing Processes for High Temperature Applications of Ni-Cr-B-Si Alloy Hardfaced on Austenitic Stainless Steel Components, *J. Mater. Res. Technol.*, 2020, **9**, p 10062–10072.
2. K. Wieczerzak, J. Michler, J.M. Wheeler, S. Lech, R. Chulist, J. Czub, A. Hoser, N. Schell, and P. Bała, An In Situ and Ex Situ Study of χ Phase Formation in a Hypoeutectic Fe-Based Hardfacing Alloy, *Mater. Des.*, 2020, **188**, p 108438.
3. J. Chen, X. Xing, Y. Wang, Y. Zhou, X. Ren, Y. Yang, and Q. Yang, Effects of Vanadium Addition on Microstructure and Tribological Performance of Bainite Hardfacing Coatings, *J. Mater. Eng. Perform.*, 2015, **24**, p 1157–1164.

4. K. Günther and J.P. Bergmann, Influencing Microstructure of Vanadium Carbide Reinforced FeCrVC Hardfacing during Gas Metal Arc Welding, *Metals.*, 2020, **10**, p 1345.

5. S. Pawar, A.K. Jha, and G. Mukhopadhyay, Effect of Different Carbides on the Wear Resistance of Fe-Based Hardfacing Alloys, *Int. J. Refract. Met. Hard. Mater.*, 2019, **78**, p 288–295.

6. M. Rafiei, H. Ghayour, H. Mostaan, and M.Z. Hosseini, The Effect of V Addition on Microstructure and Tribological Properties of Fe-Ti-C Claddings Produced by Gas Tungsten Arc Welding, *J. Mater. Process. Technol.*, 2019, **266**, p 569–578.

7. J. Wang, X. Xing, Y. Zhou, S. Liu, X. Qi, and Q. Yang, Formation Mechanism of Ultrafine M_7C_3 Carbide in a Hypereutectic Fe-25Cr-4C-0.5 Ti-0.5 Nb-0.2 N-2LaAlO3 Hardfacing Alloy Layer, *J. Mater. Res. Technol.*, 2020, **9**, p 7711–7720.

8. A. Saadat, M.K.G. Shiran, K. Amini, H. Bakhtiari, and B. Samimi, Effect of Molybdenum on Metallurgical and Wear Properties of Fe-Cr-C Hard Facing Alloy, *Prot. Met. Phys. Chem. Surf.*, 2019, **55**, p 942–950.

9. M. Roostaei, H. Aghajani, M. Abbasi, and B. Abasht, Formation of Al2O3/MoS2 Nanocomposite Coatings by the Use of Electro Spark Deposition and Oxidation, *Ceram. Int.*, 2021, **47**(8), p 11644–11653.

10. M.R. Akbarpour, N. Sadeghi, and H. Aghajani, Nano TiC-Graphene-Cu Composites Fabrication by a Modified Ball-Milling Method Followed by Reactive Sintering: Effects of Reinforcements Content on Microstructure, Consolidation, and Mechanical Properties, *Ceram. Int.*, 2022, **48**(1), p 130–136.

11. M. Jiang, Z.X. Li, Y.J. Wang, Y.W. Shi, J.M. Jiang, and X.B. Li, Effect of Vanadium on Microstructures and Properties of Fe-Cr-C Self-Shielded Metal Cored Hardfacing Alloys, *Sci. Technol. Weld. Join.*, 2008, **13**, p 114–117.

12. X. Qi, Z. Jia, Q. Yang, and Y. Yang, Effects of Vanadium Additive on Structure Property and Tribological Performance of High Chromium Cast Iron Hardfacing Metal, *Surf. Coat. Technol.*, 2011, **205**, p 5510–5514.

13. Y.K. Singla, D.K. Dwivedi, and N. Arora, On the Modeling of Dry Sliding Adhesive Wear Parameters of Vanadium Additive Iron-Based Alloys at Elevated Temperatures, *Surf. Coat. Technol.*, 2015, **283**, p 223–233.

14. H.H. Lai, C.C. Hsieh, C.M. Lin, and W. Wu, Effects of Vanadium Content on the Microstructure and Dry Sand Abrasive Wear of a Eutectic Cr-Fe-C Hardfacing Alloy, *Met. Mater. Int.*, 2016, **22**, p 101–107.

15. L. Wu, T. Yao, Y. Wang, J. Zhang, F. Xiao, and B. Liao, Understanding the Mechanical Properties of Vanadium Carbides: Nano-Indentation Measurement and First-Principles Calculations, *J. Alloys Compd.*, 2013, **548**, p 60–64.

16. V. Raghavan, C-Cr-Fe (Carbon-Chromium-Iron), *J. Phase Equilib.*, 1994, **15**, p 418–419.

17. H. Deng, H. Shi, and S. Tsuruoka, Influence of Coating Thickness and Temperature on Mechanical Properties of Steel Deposited with Co-Based Alloy Hardfacing Coating, *Surf. Coat. Tech.*, 2010, **204**, p 3927–3934.

18. L. Rovatti, J. N. Lemke, N. O. R. A. Lecis, O. Stejskal, and M. Vedani, Effect of Dilution on Microstructure and Wear Resistance of a Fe-Based Hardfacing Alloy with a High Amount of Carbide-Forming Elements. Conference Papers in Science, 2015, Article ID 276374, Hindawi

19. M. Singh, M. Majid, M.A. Akhtar, H. Arora, and K. Chawla, Wear Behaviour of SMAW Hardfaced Mild Steel and Influence of Dilution Upon Hardfacing Properties, *Int. J. Mech. Eng. Technol.*, 2017, **8**, p 1652.

20. B. Srikarun and P. Muangjunburee, The Effect of Iron-Based Hardfacing with Chromium Powder Addition Onto Low Carbon Steel, *Mater Today Proc.*, 2018, **5**, p 9272–9280.

21. H. Wang, S.F. Yu, A.R. Khan, and A.G. Huang, Effects of Vanadium on Microstructure and Wear Resistance of High Chromium Cast Iron Hardfacing Layer by Electroslag Surfacing, *Metals*, 2018, **8**, p 458.

22. H. Sabet, S. Khierandish, S. Mirdamadi, and M. Goodarzi, The Microstructure and Abrasive Wear Resistance of Fe-Cr-C Hardfacing Alloys with the Composition of Hypoeutectic, Eutectic, and Hypereutectic at Cr/C = 6, *Tribol. Lett.*, 2011, **44**, p 237–245.

23. H. Durmuş, N. Çömez, and C. Gül, M. Yurddaşkal and M. Yurddaşkal, Wear Performance of Fe-Cr-CB Hardfacing Coatings: Dry Sand/ Rubber Wheel Test and Ball-On-Disc Test, *Int. J. Refract. Met. Hard. Mater.*, 2018, **77**, p 37–43.

24. A. Cruz-Crespo, R. Fernández-Fuentes, A.V. Ferraressi, R.A. Gonçalves, and A. Scotti, Microstructure and Abrasion Resistance Of Fe-Cr-C and Fe-Cr-C-Nb Hardfacing Alloys Deposited by S-FCAW and Cold Solid Wires, *Soldagem Inspeção*, 2016, **21**, p 342–353.

25. Y.F. Zhou, Y.L. Yang, D. Li, J. Yang, Y.W. Jiang, X.J. Ren, and Q.X. Yang, Effect of Titanium Content on Microstructure and Wear Resistance of Fe-Cr-C Hardfacing Layers, *Weld. J.*, 2012, **91**, p 229–235.

26. R. Chotěborský, P. Hrabě, M. Müller, J. Savková, and M. Jirka, Abrasive Wear of High Chromium Fe-Cr-C Hardfacing Alloys, *Res. Agric. Eng.*, 2008, **54**, p 192–198.

27. A. Królicka, Ł Szczepański, Ł Konat, T. Stawicki, and P. Kostencki, The Influence of Microstructure on Abrasive Wear Micro-Mechanisms of the Claddings Produced by Welding Used in Agricultural Soil, *Materials*, 2020, **13**, p 1920.

28. K. Wang and D. Li, Formation of Core (M_7C_3)-Shell $(M_{23}C_6)$ Structured Carbides in White Cast Irons: A Thermo-Kinetic Analysis, *Comput. Mater. Sci.*, 2018, **154**, p 111–121.

29. A.T. Tabrizi, H. Aghajani, H. Saghafian, and F.F. Laleh, Correction of Archard Equation for Wear Behavior of Modified Pure Titanium, *Tribol. Int.*, 2021, **155**, p 106772.

30. Q. Wang and X. Li, Effects of Nb, V, and W on Microstructure and Abrasion Resistance of Fe-Cr-C Hardfacing Alloys, *Weld. J.*, 2010, **89**, p 133–139.

31. B. Venkatesh, K. Sriker, and V.S.V. Prabhakar, Wear characteristics of Hardfacing Alloys: State-of-the-Art, *Procedia. Mater. Sci.*, 2015, **10**, p 527–532.

32. B. Nedeljković, V. Lazić, S. Aleksandrović, B. Krstić, M. Mutavdžić, D. Milosavljević, and M. Đorđević, Influence of the Carbide Type on Tribological Properties of the Hard Faced Layers, *Metalurgija-J. Metall*, 2010, **16**, p 77–90.

33. A.T. Tabrizi, H. Aghajani, and F.F. Laleh, Tribological Characterization of Hybrid Chromium Nitride Thin Layer Synthesized on Titanium, *Surf. Coat. Technol.*, 2021, **419**, p 127317.

34. A. Günen, M. Kalkandelen, İH. Karahan, B. Kurt, E. Kanca, M.S. Gök, and S.M. Karakaş, Properties and Corrosion Behavior of Chromium and Vanadium Carbide Composite Coatings Produced on Ductile Cast Iron by Thermoreactive Diffusion Technique, *J. Eng. Mater. Technol.*, 2020, **142**, p 041008.

35. Z. Ahmad, Basic Concepts in Corrosion, in *Principles of Corrosion Engineering and Corrosion Control*. Elsevier, Chapter 2, 2006, pp. 9–56

36. Y. Toshev, V. Mandova, N. Boshkov, D. Stoychev, P. Petrov, N. Tsvetkova, G. Raichevski, Ch. Tsvetanov, A. Gabev, R. Velev, and K. Kostadinov, Protective Coating of Zinc and Zinc Alloys for Industrial Applications, in *4M 2006-Second International Conference on Multi-Material Micro Manufacture*, (Elsevier, 2006), pp. 323–326

37. E. Kocaman, B. Kılınç, M. Durmaz, Ş Şen, and U. Şen, The Influence of Chromium Content on Wear and Corrosion Behavior of Surface Alloyed Steel With Fe (16–*x*) Cr*x* (B, C) 4 electrode, *Eng. Sci. Technol. Int. J.*, 2021, **24**, p 533.

38. A.F. Zhang, J.D. Xing, L. Fang, and J.Y. Su, Inter-Phase Corrosion of Chromium White Cast Irons in Dynamic State, *Wear*, 2004, **257**, p 198–204.

39. G. Azimi and M. Shamanian, Effects of Silicon Content on the Microstructure and Corrosion Behavior of Fe-Cr-C Hardfacing Alloys, *J. Alloys. Compd.*, 2010, **505**, p 598–603.

40. C.M. Chang, C.C. Hsieh, C.M. Lin, J.H. Chen, C.M. Fan, and W. Wu, Effect of Carbon Content on Microstructure and Corrosion Behavior of Hypereutectic Fe-Cr-C Claddings, *Mater. Chem. Phys.*, 2010, **123**, p 241–246.

41. J. Gou, Y. Wang, X. Li, and F. Zhou, Effect of Rare Earth Oxide Nano-Additives on the Corrosion Behavior of Fe-Based Hardfacing Alloys in Acid, Near-Neutral and Alkaline 3.5 wt.% NaCl Solutions, *Appl. Surf. Sci.*, 2018, **431**, p 143–151.

42. A. Bedolla-Jacuinde, B. Hernández, and L. Béjar-Gómez, SEM Study on the M7C3 Carbide Nucleation during Eutectic Solidification of High-Chromium White Irons, *Zeitschrift fur Metallkunde*, 2005, **96**, p 1380–1385.

43. T. Epicier, D. Acevedo-Reyes, and M. Perez, Crystallographic Structure of Vanadium Carbide Precipitates in a Model Fe-C-V Steel, *Philos. Mag.*, 2008, **88**, p 31–45.

44. A. Ganguly, V. Murthy, and K. Kannoorpatti, Structural and Electronic Properties of Chromium Carbides and Fe-Substituted Chromium Carbides, *Mater. Res. Express*, 2020, **7**, p 056508.

45. B.J. Demaske, A. Chernatynskiy, and S.R. Phillpot, Energetics and Kinetics of Metal Impurities in the Low-Temperature Ordered Phase of V2C from First-Principles Calculations, *J. Nucl. Mater.*, 2019, **513**, p 185–191.

46. H. Altun and S. Sen, The Effect of PVD Coatings on the Corrosion Behaviour of AZ91 Magnesium Alloy, *Mater. Des.*, 2006, **27**, p 1174–1179.